Electronic Supplementary Material (ESI) for Journal of Materials Chemistry C.

Skin-like Copper/Carbon Nanotubes/Graphene Composites and the Low Thermogenesis during Electromagnetic Interference Shielding

Haizhou Liu, Ying Xu, Kang Yang, Haiyang Yong, Yan Huang, Dong Han, Xiuping Hong, Qiaowen Yang

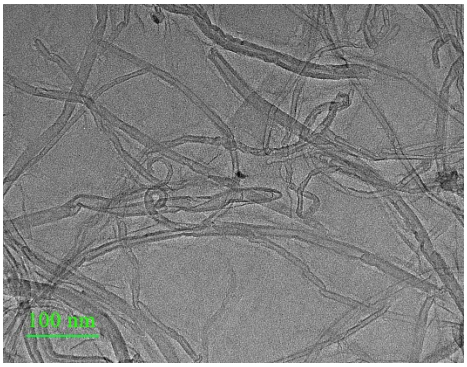

Fig. S1. TEM image of the CNTs dispersed in GO.

S1 EMI of CGP

It is well known that the electrical conductivity is a key factor affecting the EMI SE of the material[1, 2]. We first characterized the electrical conductivity of CGP with different CNTs content, as shown in Fig. S2a. Although the electrical conductivity of graphene materials prepared by the Zn reduction method has been characterized in previous article, unsurprisingly, the electrical conductivity of CGP with a dense structure was further improved. This is because GO is reduced to rGO, which removes the oxygen-containing functional groups that hinder the transport of electrons, enabling electrons to flow smoothly inside the material. Not only that, the densely interconnected structure reduces the difficulty of electron transport between adjacent sheets, which is also an important factor for the excellent electrical conductivity of CGP. In addition, it can be seen from Fig. S2a that the electrical conductivity was further improved with the addition of CNTs, and was significantly positively correlated with the content of CNTs. The electrical conductivity of CGP with 5 wt% CNTs was 0.63×10^4 $S\cdot m^{-1}$, 77.0% higher than that of

pure GP. The electrical conductivity of CGP with 15 wt% CNTs further increased to 2.65×10^4 S·m^{-1}, and that of CGP with 20 wt% CNTs reached 2.70×10^4 S·m^{-1}. As the CNTs with one-dimensional structure not only provide more electrons for the material, but also build bridges for electron transmission in the gaps of sheeted rGO, thus significantly improving the electrical conductivity. However, it is worth noting that the increase amplitude and increase slope of electrical conductivity decrease when the CNTs content in the composite exceeds 15 wt% (as shown in Fig. S2b), as it may beyond the ability of GO to disperse CNTs in this case. At this point, further increasing the CNTs content will aggregate them, which does little to improve the conductivity of the materials.

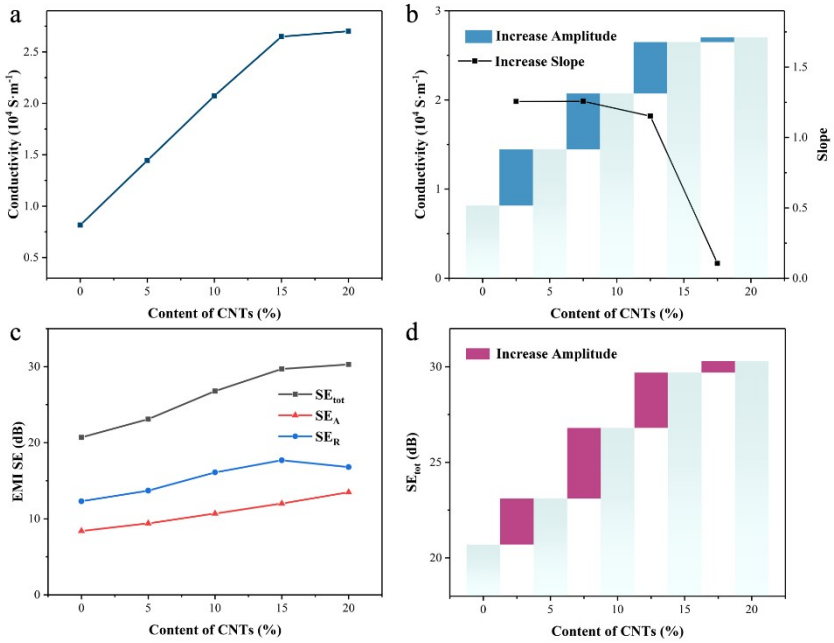

Fig. S2. The change of (a) electrical conductivity and (b) its increase amplitude and slope with CNTs content. (c) The EMI SE of CGP with different content of CNTs at 8.2 GHz. (d) The increase amplitude of EMI SE with the increase of CNTs content.

Furthermore, Fig. S2c shows the EMI SE test results of the CGP with different CNTs content. As can be seen that the changing trend of EMI SE for CGP was positively

correlated with the content of CNTs. The SE_{tot} of the GP is only 22.1 dB at 8.2 GHz, but that of CGP with 5 wt% CNTs increased to 23.1 dB, by 11.6%. The SE_{tot} of CGP with 15 wt% CNTs has been further reached 29.7 dB. We learned that the electrical conductivity of the composites has been significantly improved due to the addition of CNTs, which allows a large quantity of EMWs to be reflected when they hit the composites under the high impedance mismatch, thus playing EMI shielding. In addition, a part of the EMWs were converted into heat and absorbed under the action of electromagnetic induction and Ohm. Unfortunately, although the SE_{tot} of CGP with 20 wt% CNTs reached 30.3 dB, the increase in EMI SE was significantly reduced when the content of CNTs exceeded 15 wt% (Fig. S2d). This is also related to the agglomeration of CNTs. We have already explained the reason for the decrease in its growth rate when conducting the electrical conductivity analysis of CGP, which is still adapted here. The agglomerated CNTs did not provide additional pathways for electron transport, resulting in no further enhancement of the impedance mismatch between CGP and air, and thus the EMI SE did not further increase. In summary, the content of CNTs was selected to be 15 wt% for CGP prepared in this paper.

S2 The skin effect of CGP

The EMWs radiation at high frequencies penetrate only the near-surface region of an electrically conducting material. This phenomenon is known as skin effect. The depth, at which field drops to 1/e of the incident value is called as skin depth[3, 4] and expressed as:

$$\delta=(2/(f\mu\sigma)\text{^}(1/2)=-8.68(t/(-SE_A)) \quad (1)$$

where f is frequency, σ is electrical conductivity, μ is permeability, and t is the thickness of materials. The skin depths of GP and CGP are 11.84 μm and 10.13 μm, respectively, calculated by Equation (1).

S3 The Mechanical Property of MCGP

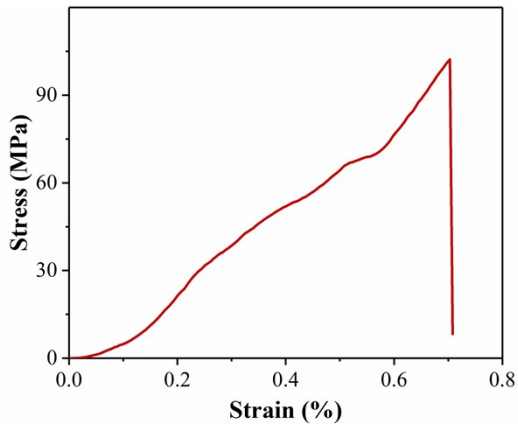

Fig. S3. Stress-strain curves of MCGP.

Flexibility is a basic mechanical property of most film/paper materials, and MCGP is no exception. As shown in Fig. S4a and b, after folding the MCGP into a diamond shape, it can be unfolded again and remains intact. Besides, the MCGP is placed in two layers of polyethylene terephthalate (PET) film (Fig. S4c), and after repeated bending (Fig. S4d), the EMI shielding test is performed, the results are shown in Fig. S4e. It is found that EMI SE was virtually unchanged before and after bending. After 100 times of bending, the SE_{tot} of MCGP is still as high as 33.7 dB, a decrease of only 5.87 % compared with the original 35.8 dB. Moreover, the SE_R and R of MCGP remain unchanged and can still reach 20.4 dB and 0.99008. This is because the compressed MCGP forms a dense structure that allows originally dispersed graphene sheets to overlap each other, with the structure similar to stacking the two books page by page. When the MCGP is bent, the van der Waals forces and π-π interaction between each layer keep the MCGP in its original structure, the mechanism is shown in Fig. S5. The excellent flexibility gives

MCGP great potential in EMI shielding of smart wearable devices such as clothing.

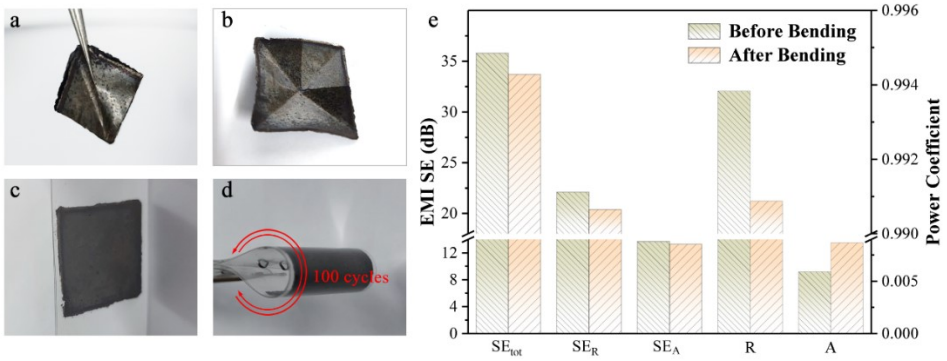

Fig. S4. Digital photos of MCGP (a) folded and then (b) stretched naturally. Digital Photos of MCGP (c) clamping with PET films and (d) bending experiment. (e) EMI SE and power coefficient of MCGP at 8.2 GHz before and after 100 bends.

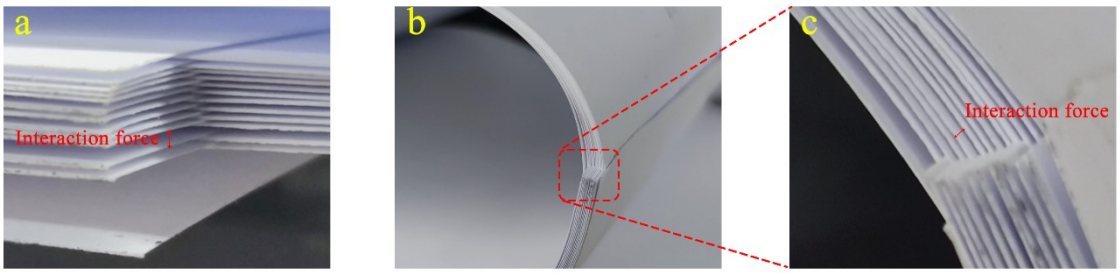

Fig. S5. Schematic diagram of MCGP structure during bending.

S4 Specific calculation methods of Temperature Rise Rate

When the EMWs knock the EMI shielding materials, it will be divided into three parts: reflected waves, absorbed waves and transmitted waves. The absorbed waves are those absorbed by the EMI material, that are eventually converted into heat energy[5, 6]. After the EMWs are absorbed by the material, it will cause the temperature of the material to rise, which is called thermogenesis phenomenon. In this study, the rate of temperature rise (T_R) was used to characterize the thermogenesis. T_R is related to the power density of the electromagnetic radiation received, and also to the electromagnetic energy absorption efficiency (E_{ae}) of the EMI shielding materials.

In this paper, the E_{ae} for the composites was calculated by equation (S1),

$$E_{ea} = P \cdot A \tag{S1}$$

The T_R for the composites was calculated by equation (S2),

$$T_R = \frac{P \cdot A}{h \cdot \rho \cdot C} \tag{S2}$$

the units of T_R is °C·min^{-1}, P is the power density of electromagnetic radiation (W·m^{-2}), A is the absorption coefficient, h is the thickness of the material (m), ρ is density (g·cm^{-3}), C is specific heat capacity (kJ·kg^{-1}·°C^{-1}).

Note: For the convenience of calculation, the heat loss of shielding materials in the environment, such as heat radiation, heat convection, etc., is not considered.

In this study, the T_R for the shielding material after absorbing EMWs is calculated under the power of the common microwave emitting source. In the calculation, it is assumed that a microwave source with a transmission power of 600 W emits EMWs uniformly in 6 directions, and the power density at 1 m^2 in each direction is 100 W·m^{-2}, as shown in Fig. S6. Besides, PDMS was used as a composite matrix with a density of 1.21 g·cm^{-3} and a specific heat capacity of 1.38 kJ·kg^{-1}·°C^{-17}. The structure schematics of the MCGP/PDMS and CF/PDMS and their dimensions for simulation calculation are shown in Fig. S7. The parameters used to calculate the T_R of MCGP/PDMS, CF/PDMS and MCGP/CF/PDMS are shown in Table S1.

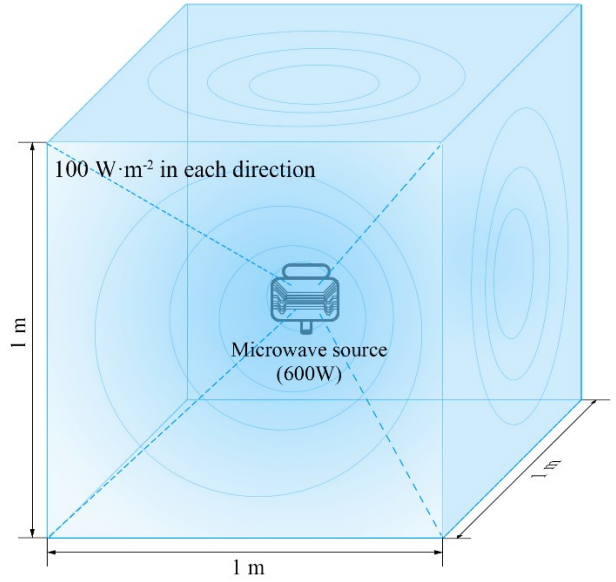

Fig. S6. Schematic diagram of microwave source transmitting power segmentation.

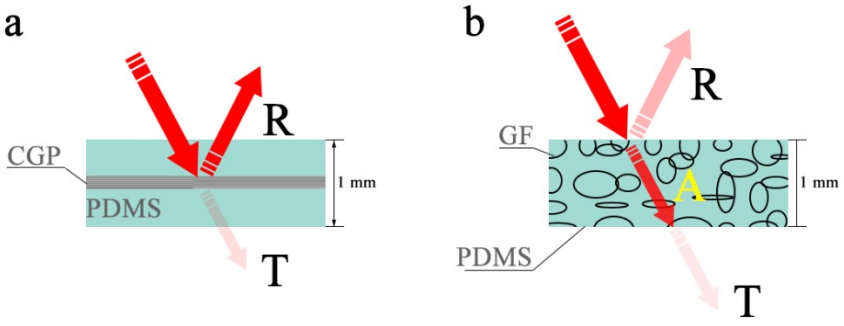

Fig. S7. The structure schematics of the (a) MCGP/PDMS and (b) CF/PDMS and their dimensions for simulation calculation.

Table S1. The parameters used to calculate T_R for MCGP/PDMS and other samples.

P ($W \cdot m^{-2}$)	h (mm)	ρ ($g \cdot cm^{-3}$)	C ($kJ \cdot kg^{-1} \cdot °C^{-1}$)
100 50	1.0	1.21	1.38

Table S2. The EMI SE of different samples and its theoretical E_{ae}, T_R and the time required to rise by 1 ° C at 100 $W \cdot m^{-2}$.

Samples	EMI SE	E_{ae}	T_R	Time

	(dB)	($W \cdot m^{-2}$)	($°C \cdot min^{-1}$)	(min)
MCGP	35.8	0.59	0.021	47
MGP	27.0	1.53	0.055	18
CGP	29.7	1.59	0.057	17
GP	22.1	4.06	0.146	7
CF	34.1	21.34	1.109	0.9
MCGP/CF (PS)	70.2	0.34	0.012	83
MCGP/CF (FS)	66.4	11.7	0.422	2.4

References:

1. E. Zhou, J. Xi, Y. Guo, Y. Liu, Z. Xu, L. Peng, W. Gao, J. Ying, Z. Chen and C. Gao, *Carbon*, 2018, **133**, 316-322.
2. C. Liang, P. Song, H. Qiu, Y. Huangfu, Y. Lu, L. Wang, J. Kong and J. Gu, *Composites Part A: Applied Science and Manufacturing*, 2019, **124**.
3. A. Chaudhary, S. Kumari, R. Kumar, S. Teotia, B. P. Singh, A. P. Singh, S. K. Dhawan and S. R. Dhakate, *ACS Appl Mater Interfaces*, 2016, **8**, 10600-10608.
4. H. Liu, Y. Xu, X. Zhao, D. Han, F. Zhao and Q. Yang, *Carbon*, 2022, **191**, 183-194.
5. H. L. Lv, Z. H. Yang, H. G. Pan and R. B. Wu, *Prog. Mater. Sci.*, 2022, **127**, 74.
6. H. S. Choe, J. S. Lee, J. H. Kweon, Y. W. Nam and W. H. Choi, *Compos. Struct.*, 2022, **283**, 13.
7. P. Yi, R. A. Awang, W. S. Rowe, K. Kalantar-zadeh and K. Khoshmanesh, *Lab Chip*, 2014, **14**, 3419-3426.